

# UNIVERSITY OF BIRMINGHAM

## Research at Birmingham

### Induction and transcriptional regulation of the co-inhibitory gene module in T cells

Chihara, Norio; Buckley, Christopher

*DOI:*

[10.1038/s41586-018-0206-z](https://doi.org/10.1038/s41586-018-0206-z)

*License:*

None: All rights reserved

*Document Version*

Peer reviewed version

*Citation for published version (Harvard):*

Chihara, N & Buckley, C 2018, 'Induction and transcriptional regulation of the co-inhibitory gene module in T cells', *Nature*, vol. 558, pp. 454–459. <https://doi.org/10.1038/s41586-018-0206-z>

[Link to publication on Research at Birmingham portal](#)

**Publisher Rights Statement:**

Final version of record available at: <https://doi.org/10.1038/s41586-018-0206-z>

Checked for eligibility: 01/05/2018

**General rights**

Unless a licence is specified above, all rights (including copyright and moral rights) in this document are retained by the authors and/or the copyright holders. The express permission of the copyright holder must be obtained for any use of this material other than for purposes permitted by law.

- Users may freely distribute the URL that is used to identify this publication.
- Users may download and/or print one copy of the publication from the University of Birmingham research portal for the purpose of private study or non-commercial research.
- User may use extracts from the document in line with the concept of 'fair dealing' under the Copyright, Designs and Patents Act 1988 (?)
- Users may not further distribute the material nor use it for the purposes of commercial gain.

Where a licence is displayed above, please note the terms and conditions of the licence govern your use of this document.

When citing, please reference the published version.

**Take down policy**

While the University of Birmingham exercises care and attention in making items available there are rare occasions when an item has been uploaded in error or has been deemed to be commercially or otherwise sensitive.

If you believe that this is the case for this document, please contact [UBIRA@lists.bham.ac.uk](mailto:UBIRA@lists.bham.ac.uk) providing details and we will remove access to the work immediately and investigate.

1 **Induction and transcriptional regulation of the co-inhibitory gene module in T cells**

2

3 Norio Chihara<sup>1,\*</sup>, Asaf Madi<sup>1,\*</sup>, Takaaki Kondo<sup>1</sup>, Huiyuan Zhang<sup>1</sup>, Nandini Acharya<sup>1</sup>,  
4 Meromit Singer<sup>2</sup>, Jackson Nyman<sup>2</sup>, Nemanja D. Marjanovic<sup>2</sup>, Monika S. Kowalczyk<sup>2</sup>,  
5 Chao Wang<sup>1</sup>, Sema Kurtulus<sup>1</sup>, Travis Law<sup>2</sup>, Yasaman Etminan<sup>1</sup>, James Nevin<sup>1</sup>,  
6 Christopher D. Buckley<sup>3</sup>, Patrick R. Burkett<sup>1,4</sup>, Jason D. Buenrostro<sup>2</sup>, Orit Rozenblatt-  
7 Rosen<sup>2</sup>, Ana C. Anderson<sup>1,2,†,§</sup>, Aviv Regev<sup>2,5,6,†,§</sup>, Vijay K. Kuchroo<sup>1,2,†,§</sup>

8

9 <sup>1</sup>Evergrande Center for Immunologic Diseases and Ann Romney Center for Neurologic  
10 Diseases, Harvard Medical School and Brigham and Women's Hospital, Boston, MA  
11 02115, <sup>2</sup>Broad Institute of MIT and Harvard, Cambridge, MA 02142, <sup>3</sup>Rheumatology  
12 Research Group, Center for Translational Inflammation Research, Queen Elizabeth  
13 Hospital, Birmingham, United Kingdom. <sup>4</sup>Pulmonary and Critical Care Division,  
14 Department of Medicine, Brigham and Women's Hospital, <sup>5</sup>Howard Hughes Medical  
15 Institute, <sup>6</sup>Department of Biology, Koch Institute and Ludwig Center, Massachusetts  
16 Institute of Technology, Cambridge, MA 02142.

17

18 \* Co-first author

19 † Co-senior author

20

21 **§Correspondence:** vkuchroo@evergrande.hms.harvard.edu (V.K.K.),

22 aregev@broadinstitute.org (A.R.), acanderson@partners.org (A.C.A.)

23

24

25 **Abstract**

26 Expression of co-inhibitory receptors, such as CTLA-4 and PD-1, on effector T cells is a  
27 key mechanism for ensuring immune homeostasis. Dysregulated co-inhibitory receptor  
28 expression on CD4<sup>+</sup> T cells promotes autoimmunity while sustained overexpression on  
29 CD8<sup>+</sup> T cells promotes T cell dysfunction or exhaustion, leading to impaired ability to  
30 clear chronic viral infections and cancer<sup>1,2</sup>. Here, we used RNA and protein expression  
31 profiling at single-cell resolution to identify a module of co-inhibitory receptors that  
32 includes not only several known co-inhibitory receptors (PD-1, Tim-3, Lag-3, and  
33 TIGIT), but also a number of novel surface receptors. We functionally validated two  
34 novel co-inhibitory receptors, Activated protein C receptor (Procr) and Podoplanin  
35 (Pdpn). The module of co-inhibitory receptors is co-expressed in both CD4<sup>+</sup> and CD8<sup>+</sup> T  
36 cells and is part of a larger co-inhibitory gene program that is shared by non-responsive T  
37 cells in multiple physiological contexts and is driven by the immunoregulatory cytokine  
38 IL-27. Computational analysis identified the transcription factors Prdm1 and c-Maf as  
39 cooperative regulators of the co-inhibitory module, which we validated experimentally.  
40 This molecular circuit underlies the co-expression of co-inhibitory receptors in T cells  
41 and identifies novel regulators of T cell function with the potential to regulate  
42 autoimmunity and tumor immunity.  
43

44 We used single-cell RNA-seq (scRNA-Seq) to analyze co-inhibitory and co-  
45 stimulatory receptor expression in 588 CD8<sup>+</sup> and 316 CD4<sup>+</sup> tumor-infiltrating  
46 lymphocytes (TILs) from B16F10 melanoma<sup>3</sup>. We found that PD-1, Tim-3, Lag-3,  
47 CTLA-4, 4-1BB, and TIGIT strongly co-vary in CD8<sup>+</sup> TILs. CD4<sup>+</sup> TILs showed a similar  
48 pattern with the additional co-expression of ICOS, GITR, and OX40 (**Fig. 1a, top**).  
49 Single-cell mass cytometry (CyTOF) confirmed the surface co-expression of these  
50 receptors (**Fig. 1a, bottom, Supplementary Table Information 1**). Expression of PD-1,  
51 Lag-3, Tim-3, and TIGIT was tightly correlated on both CD8<sup>+</sup> and CD4<sup>+</sup> TILs (**Fig. 1a,**  
52 **bottom**). Clustering analysis (t-SNE<sup>4</sup>, **Methods**) showed two groups of CD8<sup>+</sup> TILs  
53 (clusters 1 and 2) (**Fig. 1b, Extended Data Fig. 1a,c**) where PD-1, Lag-3, Tim-3, and  
54 TIGIT were mainly expressed in cluster 1 cells (**Fig. 1b, Extended Data Fig. 1c**) as were  
55 LILRB4 (**Extended Data Fig. 1a**), and co-stimulatory receptors of the TNF-receptor  
56 family, 4-1BB, OX-40, and GITR. In contrast, ICOS and CD226 were less restricted to  
57 cluster 1 (**Extended Data Fig. 1a**). We further observed two discrete clusters of CD4<sup>+</sup>  
58 TILs (clusters 3 and 4) wherein PD-1, Tim-3, Lag-3, and TIGIT co-expression was  
59 restricted to cluster 3 (**Fig. 1b, Extended Data Fig. 1c**).

60 The co-expression of co-inhibitory receptors on CD8<sup>+</sup> and CD4<sup>+</sup> T cells suggests  
61 a common trigger. One candidate is IL-27, a heterodimeric member of the IL-12 cytokine  
62 family that suppresses autoimmunity<sup>5</sup>, induces IL-10-secreting Type 1 regulatory (Tr1)  
63 cells<sup>6,7</sup>, and induces expression of Tim-3 and PD-L1 on CD4<sup>+</sup> and CD8<sup>+</sup> T cells<sup>8,9</sup>.  
64 Activation of CD4<sup>+</sup> and CD8<sup>+</sup> T cells in the presence of IL-27 induced Tim-3 (Havcr2),  
65 Lag-3, and TIGIT at mRNA (**Fig. 1c**) and protein levels (**Extended Data Fig. 2a**).  
66 Expression of Tim-3, Lag-3, and TIGIT was reduced in IL-27R-deficient T cells, whereas

67 PD-1 (*Pdcd1*) expression was unaffected by IL-27 *in vitro* (**Fig. 1c, Extended Data Fig.**  
68 **2a**).

69 CyTOF analysis showed that loss of IL-27ra resulted in loss of cells in cluster 1 of  
70 CD8<sup>+</sup> TILs and cluster 3 of CD4<sup>+</sup> TILs (**Fig. 1d**, p-value=  $5 \times 10^{-23}$  and  $6.8 \times 10^{-7}$  for CD8<sup>+</sup>  
71 and CD4<sup>+</sup> respectively, hypergeometric test, **Extended Data Fig. 1b,c,d**), indicating a  
72 key role for IL-27 in driving co-inhibitory receptor co-expression in both CD4<sup>+</sup> and CD8<sup>+</sup>  
73 T cells *in vivo*. Although PD-1 expression wasn't dependent on IL-27 *in vitro*, it was  
74 dependent on IL-27R signaling *in vivo*. In line with the induction of IL-10 by IL-27<sup>5-7</sup>, we  
75 observed reduced IL-10 in IL27ra KO CD8<sup>+</sup> TILs (**Extended Data Fig. 2b**).

76 scRNA-seq of CD8<sup>+</sup> and CD4<sup>+</sup> TILs from WT and IL27ra KO mice (**Fig. 1e**,  
77 **Extended Data Fig. 3a,b; Methods**) revealed distinct clusters of CD8<sup>+</sup> (cluster 5) and  
78 CD4<sup>+</sup> (cluster 4) TILs that highly expressed the co-inhibitory receptors PD-1, Tim-3,  
79 Lag-3, and TIGIT. Expression of these genes was decreased in CD8<sup>+</sup> TILs from IL27ra  
80 KO mice, while only Tim-3 and Lag-3 were decreased in CD4<sup>+</sup> TILs from IL27ra KO  
81 mice (**Fig. 1e**). Thus, IL-27 drives a module of co-inhibitory receptors that are strongly  
82 co-expressed *in vivo* together with IL-10.

83 The co-inhibitory receptor module could be part of a larger IL-27-driven  
84 inhibitory gene program. We analyzed the mRNA profiles of CD4<sup>+</sup> and CD8<sup>+</sup> T cells  
85 stimulated in the presence or absence of IL-27. IL-27 induced similar expression  
86 programs in CD4<sup>+</sup> and CD8<sup>+</sup> T cells (**Extended Data Fig. 4a,b**). We identified 1,201  
87 genes with IL-27-dependent expression (**Methods**). We compared the IL-27-driven gene  
88 program to the gene signatures for four different states of T cell non-responsiveness:  
89 CD8<sup>+</sup> T cell exhaustion in both cancer<sup>3</sup> and chronic viral infection<sup>10</sup> and antigen-

90 specific<sup>11</sup> or non-specific (anti-CD3 antibody<sup>12</sup>) CD4<sup>+</sup> T cell tolerance. We found  
91 significant overlap with all of these signatures (**Methods, Extended Data Fig. 4c-f**).

92 Projection of the IL-27/CD8<sup>+</sup> cancer T cell exhaustion overlap signature onto the  
93 single-cell profiles of CD8<sup>+</sup> TILs marked a distinct subset of cells (**Fig. 2a**, panel I). This  
94 subset scored highly for the overlap signatures between the IL-27-driven gene program  
95 and each of the other three states of T cell non-responsiveness (**Fig. 2a**, panels II-IV).  
96 The transcriptional program induced in IL27ra KO TILs was active in a complimentary  
97 subset of TILs (**Methods, Fig. 2a** panel V). The control signature from cells stimulated  
98 with IL-27 *in vitro* showed bimodal distribution and by itself did not detect the same  
99 population of cells (**Fig. 2a** panel VI). From these analyses, we identified a co-inhibitory  
100 gene module (272 genes) that is shared across multiple states of T cell non-  
101 responsiveness (**Supplementary Information Table 2**). Within this module, we  
102 identified a set of 57 genes encoding cell surface receptors and cytokines, including Tim-  
103 3, Lag-3, TIGIT, and IL10 (**Fig. 2b**), which we further stratified by their expression in  
104 cancer and chronic viral infections (**Fig. 2c**). Two surface molecules, Procr (protein C  
105 receptor) and Pdpn (podoplanin) were highly expressed in the setting of cancer (**Fig. 2c**).  
106 Activation of naïve CD4<sup>+</sup> and CD8<sup>+</sup> T cells *in vitro* in the presence of IL-27 induced the  
107 expression of Procr and Pdpn (**Extended Data Fig. 5a**). *In vivo*, Procr and Pdpn  
108 exhibited IL-27 dependent co-expression with PD-1 and Tim-3 on CD8<sup>+</sup> TILs (**Extended**  
109 **Data Fig. 5b**).

110 Procr<sup>+</sup> CD8<sup>+</sup> TILs exhibited an exhausted phenotype, producing less TNF $\alpha$  and  
111 IL-2 and more IL-10 than Procr<sup>-</sup> CD8<sup>+</sup> TILs (**Extended Data Fig. 5c**). Growth of  
112 B16F10 melanoma was inhibited in Procr hypomorph (Procr<sup>d/d</sup>)<sup>13</sup> mice (**Fig. 2d**), and

113 Procr<sup>d/d</sup> CD8<sup>+</sup> TILs mice exhibited enhanced TNF $\alpha$  production, but no difference in IL-2,  
114 IFN- $\gamma$ , or IL-10 (**Fig. 2e**). Procr<sup>d/d</sup> TILs exhibited a decreased frequency of Tim-3<sup>hi</sup>PD-1<sup>hi</sup>  
115 CD8<sup>+</sup> T cells suggesting that Procr signaling promotes a severely exhausted phenotype in  
116 CD8<sup>+</sup> T cells<sup>14</sup> (**Fig. 2f**). Adoptive transfer of CD8<sup>+</sup> T cells lacking Procr revealed a T  
117 cell specific role for Procr in constraining tumor growth (**Extended Data Fig. 5d**).

118 Although Pdpn can limit CD4<sup>+</sup> T cell survival in inflamed tissues<sup>15</sup>, its role in T  
119 cell exhaustion is unknown. We observed a significant delay in B16F10 tumor growth in  
120 mice with Pdpn deficiency in T cells (Pdpn cKO) (**Fig. 2g**). Pdpn-deficient CD8<sup>+</sup> TILs  
121 exhibited enhanced TNF $\alpha$  production but no significant difference in IL-2, IFN- $\gamma$ , or IL-  
122 10 (**Fig. 2h**). The frequency of Tim-3<sup>hi</sup>PD-1<sup>hi</sup> CD8<sup>+</sup> TILs was decreased, indicating a  
123 reduced accumulation of T cells with a severely exhausted phenotype in Pdpn cKO<sup>14</sup>  
124 (**Fig. 2i**). Consistent with previous data<sup>15</sup>, Pdpn-deficient PD-1<sup>+</sup>Tim-3<sup>+</sup> CD8<sup>+</sup> TILs had  
125 higher expression of IL-7Ra, indicating that Pdpn may limit the survival of CD8<sup>+</sup> TILs in  
126 the tumor microenvironment (**Extended Data Fig. 5e,f**).

127 We identified the transcription factor (TF) Prdm1 as a candidate regulator of the  
128 co-inhibitory module. Prdm1 is induced *in vitro* by IL-27 in CD4<sup>+</sup> and CD8<sup>+</sup> T cells  
129 (**Extended Data Fig. 6a**), is enriched in TILs with high expression of the IL-27 co-  
130 inhibitory module (**Extended Data Fig. 3c-f** and **6b,c** and **Methods**), and is  
131 overexpressed in exhausted CD8<sup>+</sup> TILs (p-value= 0.0004, t-test, **Extended Data Fig. 6d**).  
132 Network analysis based on profiling of naïve CD8<sup>+</sup> T cells from mice with a T cell  
133 specific deletion of Prdm1 (Prdm1 cKO) stimulated with IL-27, showed that Prdm1  
134 regulates multiple genes in the IL-27 co-inhibitory module (**Extended Data Fig. 6e**, p-

135 value=  $2.32 \times 10^{-12}$ ; hypergeometric test; **Methods**). This was further supported by Prdm1  
136 Chip-seq data<sup>16</sup> (p-value=  $2.9 \times 10^{-8}$  respectively, hypergeometric test; **Fig. 6e; Methods**).

137 CD8<sup>+</sup> TILs from B16F10 tumor-bearing Prdm1 cKO mice expressed lower levels  
138 of Tim-3, PD-1, and Procr (**Fig. 3a**); however, there was no difference in tumor growth  
139 compared to wild type (WT) controls (**Fig. 3b**), indicating that the reduction of co-  
140 inhibitory receptor expression in Prdm1 cKO mice was insufficient to promote effective  
141 anti-tumor immunity. We therefore examined whether other TFs may regulate the co-  
142 inhibitory module and compensate for the absence of Prdm1. We analyzed CD8<sup>+</sup> TILs  
143 from Prdm1 cKO mice for the expression of genes from the IL-27-driven gene signature  
144 and the signature for exhausted CD8<sup>+</sup> TILs (**Methods; Supplementary Information**  
145 **Table 3**). We found that only a few genes were upregulated in Prdm-1 cKO CD8<sup>+</sup> T cells,  
146 including one TF, c-Maf (p-value < 0.05) (**Fig. 3c**). Indeed, c-Maf is induced by IL-27, is  
147 co-expressed with Prdm1 in T cells upon IL-27 stimulation (**Extended Data Fig. 6a**),  
148 and can regulate IL-10 expression<sup>17</sup> and T cell exhaustion<sup>18</sup>. Additionally, many genes  
149 (226 genes, p-value  $5.34 \times 10^{-5}$ , hypergeometric test) in the co-inhibitory gene module  
150 have a binding motif and a reported binding event for c-Maf within their promoter  
151 regions<sup>19</sup>.

152 CD8<sup>+</sup> TILs from c-Maf cKO mice exhibited decreased expression of multiple co-  
153 inhibitory receptors (**Fig. 3d**). Interestingly, Prdm1 and c-Maf each impacted co-  
154 inhibitory receptor expression only partially (**Fig. 3e**). As in the Prdm1 cKO mice, c-Maf  
155 cKO mice did not show any differences in tumor growth relative to controls (**Fig. 3f**).  
156 Notably, Prdm1 expression in c-Maf cKO TILs was similar to that in WT TILs,



157 indicating that Prdm1 might drive expression of the co-inhibitory gene module in the  
158 absence of c-Maf.

159 We addressed whether Prdm1 and c-Maf could act cooperatively to regulate co-  
160 inhibitory receptor expression. We found no evidence for a physical interaction between  
161 Prdm1 and c-Maf (data not shown); therefore we examined whether they shared targets.  
162 We combined the network analysis for Prdm1 (**Extended Data Fig. 6e**) with c-Maf  
163 ChIP-seq data<sup>19</sup> and c-Maf targets (**Methods**). We observed 121 genes in the co-  
164 inhibitory module that are affected (RNAseq) or have a direct binding event (ChIP-Seq)  
165 for both Prdm1 and c-Maf (**Fig. 4a**), but that are not affected in either individual  
166 knockout. This is consistent, among other possibilities, with compensatory (*e.g.*, “OR”)  
167 regulation<sup>20</sup>. Examination of ATACseq<sup>21,22</sup> and ChIP-seq data for PD-1, Tim-3, Lag-3  
168 and TIGIT shows that Prdm1 and c-Maf can bind both overlapping and non-overlapping  
169 sites in the loci of these receptors and can synergistically trans-activate Tim-3 expression  
170 (**Extended Data Fig. 7**).

171 Mice with a T cell specific deletion in both Prdm1 and c-Maf (Prdm1/c-Maf  
172 cDKO) showed normal development of CD4<sup>+</sup> and CD8<sup>+</sup> T cells in terms of frequency  
173 and expression of memory/activation markers, although the frequency of Foxp3<sup>+</sup> Treg  
174 was increased (**Extended Data Fig. 8a**). CD4<sup>+</sup> and CD8<sup>+</sup> TILs from cDKO mice bearing  
175 B16F10 melanomas exhibited a near absence of PD-1, Tim-3, Lag-3, TIGIT, Pdpn, and  
176 Procr expression (**Fig. 4b; Extended Data Fig. 8b**). Moreover, cDKO CD8<sup>+</sup> TILs  
177 exhibited enhanced IL-2 and TNF $\alpha$  production (**Extended Data Fig. 8c**). In contrast to  
178 singly deficient mice, cDKO mice showed significant control of B16F10 tumor growth  
179 despite the increased frequency of Treg (**Fig. 4c**). We addressed whether Prdm1 and c-

180 Maf play a cell-intrinsic role in CD8<sup>+</sup> and CD4<sup>+</sup> T cells in controlling tumor growth by  
181 using an adoptive transfer model. Although CD8<sup>+</sup> T cells from cDKO were able to inhibit  
182 tumor growth with decreased expression of co-inhibitory molecules, these effects were  
183 stronger when Prdm1 and c-Maf were lacking in both CD4<sup>+</sup> and CD8<sup>+</sup> T cells (**Fig. 4d;**  
184 **Extended Data Fig. 8d**). We examined the roles of Prdm-1 and c-Maf in tumor antigen-  
185 specific T cell responses using the MC38-OVA tumor model. We observed a significant  
186 reduction in tumor growth in mice receiving cDKO T cells as compared to mice receiving  
187 WT T cells (**Extended Data Fig. 8e**). We also observed an increase in Ova-specific T  
188 cells in the tumor draining lymph nodes and in OVA-specific IFN- $\gamma$  and TNF-  
189  $\alpha$  producing CD8<sup>+</sup> T cells in both the tumor infiltrate and in the periphery in mice  
190 receiving DKO T cells (**Fig. 4e,f; Extended Data Fig. 8f**). Lastly, we observed an  
191 increase in CD8<sup>+</sup> Ki67<sup>+</sup> T cells in the periphery of mice receiving DKO T cells (**Fig. 4f**).

192 We tested for non-additive effects between Prdm1 and c-Maf by using a binomial  
193 generalized linear model to compare the effect of single knockouts to the cDKO, and  
194 found that 149 out of 940 differentially expressed genes (adj. p-value<0.05, likelihood  
195 ratio test and FDR correction) between WT and cDKO CD8<sup>+</sup> TILs have non-additive (i.e.  
196 synergistic) effects (**Extended Data Fig. 9, Methods**).

197 Examination of the transcriptional signatures of cDKO CD8<sup>+</sup> TILs showed  
198 significant overlap with those of CD8<sup>+</sup> Tim-3<sup>-</sup>PD-1<sup>-</sup> TILs (**Fig. 4g; p-value = 2.8x10<sup>-7</sup>**  
199 one-sample Kolmogorov-Smirnov test, **Extended Data Fig. 10a-c**, p-value=0.008),  
200 suggesting that loss of both c-Maf and Prdm1 increases the proportion of non-exhausted  
201 CD8<sup>+</sup> effectors that exist normally in tumors. We scored the individual scRNA-seq  
202 profiles of CD8<sup>+</sup> TILs for the cDKO 940 gene signature and found that expression of the

203 cDKO gene signature and the co-inhibitory gene module signature mark mutually  
204 exclusive populations of TILs (**Extended Data Fig. 10e**). The cDKO signature showed  
205 significant overlap with PD-1<sup>+</sup>CXCR5<sup>+</sup>CD8<sup>+</sup> T cells, which may represent precursors for  
206 functional effectors in chronic LCMV infection<sup>23</sup> (**Extended Data Fig. 10d,e**, p-value =  
207  $1 \times 10^{-13}$  one-sample Kolmogorov-Smirnov test). Furthermore, the IL27ra KO TILs  
208 signature also showed significant overlap with this PD-1<sup>+</sup>CXCR5<sup>+</sup>CD8<sup>+</sup> T cell signature  
209 (p-value <  $2.2 \times 10^{-16}$  one-sample Kolmogorov-Smirnov test, **Extended Data Fig. 10e**;  
210 **Fig. 2a**). Collectively, our data indicate that loss of c-Maf and Prdm1 preferentially  
211 results in loss of the co-inhibitory gene module expression and acquisition of a more  
212 responsive effector T cell state.

213 In conclusion, we identified a co-inhibitory gene module, which is expressed in  
214 multiple settings of both CD4<sup>+</sup> and CD8<sup>+</sup> T cell non-responsiveness, along with its  
215 transcriptional regulators. The discovery of this module provides a basis for the  
216 identification of novel co-inhibitory and co-stimulatory receptors that may play an  
217 important role in T cell regulation.

218

## 219 **Acknowledgements**

220 We thank Mary Collins for insightful discussions, Deneen Kozoriz, Junrong Xia, and  
221 Zoujia Chen for technical advice, Samantha Riesenfeld for computational advice, Nicole  
222 Paul and Josh Keegan for CyTOF, and Leslie Gaffney for artwork. This work was  
223 supported by grants from the National Institutes of Health, the American Cancer Society,  
224 the Melanoma Research Alliance, the Klarman Cell Observatory at the Broad Institute,  
225 and the Howard Hughes Medical Institute.

226

227 **Author Contributions**

228 N.C., A.M., P.R.B., A.C.A., O.R.R., A.R. and V.K.K. designed the experiment; N.C.,  
229 A.M., S.K., J.N., C.B., P.R.B., J.D.B, and A.R. developed analytical tools; N.C., A.M.,  
230 T.K., N.A, J.N., N.D.M., M.S.K., C.W., H.Z., T.L., Y.E. and P.R.B. performed  
231 experiments; A.M. and M.S. performed computational analysis. N.C. and A.M. wrote the  
232 original draft of the paper and P.R.B., A.C.A, A.R. and V.K.K. reviewed and edited the  
233 paper; A.C.A., A.R., and V.K.K. supervised the project.

234

235 **Conflict of Interest**

236 A.C.A. is a member of the SAB for Potenza Therapeutics and Tizona Therapeutics.  
237 V.K.K. has an ownership interest and is a member of the SAB for Potenza Therapeutics  
238 and Tizona Therapeutics. A.C.A.'s and V.K.K.'s interests were reviewed and managed by  
239 the Brigham and Women's Hospital and Partners Healthcare in accordance with their  
240 conflict of interest policies. A.R. is an SAB member for Thermo Fisher and Syros  
241 Pharmaceuticals and is a consultant for Driver Group.

242

243 **References**

- 244 1 Wherry, E. J. & Kurachi, M. Molecular and cellular insights into T cell  
 245 exhaustion. *Nature reviews. Immunology* **15**, 486-499, doi:10.1038/nri3862  
 246 (2015).
- 247 2 Anderson, A. C., Joller, N. & Kuchroo, V. K. Lag-3, Tim-3, and TIGIT: Co-  
 248 inhibitory Receptors with Specialized Functions in Immune Regulation.  
 249 *Immunity* **44**, 989-1004, doi:10.1016/j.immuni.2016.05.001 (2016).
- 250 3 Singer, M. *et al.* A Distinct Gene Module for Dysfunction Uncoupled from  
 251 Activation in Tumor-Infiltrating T Cells. *Cell* **166**, 1500-1511 e1509,  
 252 doi:10.1016/j.cell.2016.08.052 (2016).
- 253 4 Maaten L, H. G. Visualizing Data using t-SNE. *Journal of Machine Learning*  
 254 *Research*, 2579-2605 (2008).
- 255 5 Fitzgerald, D. C. *et al.* Suppression of autoimmune inflammation of the central  
 256 nervous system by interleukin 10 secreted by interleukin 27-stimulated T  
 257 cells. *Nature immunology* **8**, 1372-1379, doi:10.1038/ni1540 (2007).
- 258 6 Awasthi, A. *et al.* A dominant function for interleukin 27 in generating  
 259 interleukin 10-producing anti-inflammatory T cells. *Nature immunology* **8**,  
 260 1380-1389, doi:10.1038/ni1541 (2007).
- 261 7 Stumhofer, J. S. *et al.* Interleukins 27 and 6 induce STAT3-mediated T cell  
 262 production of interleukin 10. *Nature immunology* **8**, 1363-1371,  
 263 doi:10.1038/ni1537 (2007).
- 264 8 Zhu, C. *et al.* An IL-27/NFIL3 signalling axis drives Tim-3 and IL-10  
 265 expression and T-cell dysfunction. *Nature communications* **6**, 6072,  
 266 doi:10.1038/ncomms7072 (2015).
- 267 9 Hirahara, K. *et al.* Interleukin-27 priming of T cells controls IL-17 production  
 268 in trans via induction of the ligand PD-L1. *Immunity* **36**, 1017-1030,  
 269 doi:10.1016/j.immuni.2012.03.024 (2012).
- 270 10 Doering, T. A. *et al.* Network analysis reveals centrally connected genes and  
 271 pathways involved in CD8+ T cell exhaustion versus memory. *Immunity* **37**,  
 272 1130-1144, doi:10.1016/j.immuni.2012.08.021 (2012).
- 273 11 Burton, B. R. *et al.* Sequential transcriptional changes dictate safe and  
 274 effective antigen-specific immunotherapy. *Nature communications* **5**, 4741,  
 275 doi:10.1038/ncomms5741 (2014).
- 276 12 Mayo, L. *et al.* IL-10-dependent Tr1 cells attenuate astrocyte activation and  
 277 ameliorate chronic central nervous system inflammation. *Brain*,  
 278 doi:10.1093/brain/aww113 (2016).
- 279 13 Castellino, F. J. *et al.* Mice with a severe deficiency of the endothelial protein C  
 280 receptor gene develop, survive, and reproduce normally, and do not present  
 281 with enhanced arterial thrombosis after challenge. *Thrombosis and*  
 282 *haemostasis* **88**, 462-472, doi:10.1267/THRO88030462 (2002).
- 283 14 Sakuishi, K. *et al.* Targeting Tim-3 and PD-1 pathways to reverse T cell  
 284 exhaustion and restore anti-tumor immunity. *The Journal of experimental*  
 285 *medicine* **207**, 2187-2194, doi:10.1084/jem.20100643 (2010).

- 286 15 Peters, A. *et al.* Podoplanin negatively regulates CD4+ effector T cell  
287 responses. *The Journal of clinical investigation* **125**, 129-140,  
288 doi:10.1172/JCI74685 (2015).
- 289 16 Mackay, L. K. *et al.* Hobit and Blimp1 instruct a universal transcriptional  
290 program of tissue residency in lymphocytes. *Science* **352**, 459-463,  
291 doi:10.1126/science.aad2035 (2016).
- 292 17 Apetoh, L. *et al.* The aryl hydrocarbon receptor interacts with c-Maf to  
293 promote the differentiation of type 1 regulatory T cells induced by IL-27.  
294 *Nature immunology* **11**, 854-861, doi:10.1038/ni.1912 (2010).
- 295 18 Giordano, M. *et al.* Molecular profiling of CD8 T cells in autochthonous  
296 melanoma identifies Maf as driver of exhaustion. *EMBO J* **34**, 2042-2058,  
297 doi:10.15252/embj.201490786 (2015).
- 298 19 Ciofani, M. *et al.* A validated regulatory network for Th17 cell specification.  
299 *Cell* **151**, 289-303, doi:10.1016/j.cell.2012.09.016 (2012).
- 300 20 Capaldi, A. P. *et al.* Structure and function of a transcriptional network  
301 activated by the MAPK Hog1. *Nat Genet* **40**, 1300-1306, doi:10.1038/ng.235  
302 (2008).
- 303 21 Karwacz, K. *et al.* Critical role of IRF1 and BATF in forming chromatin  
304 landscape during type 1 regulatory cell differentiation. *Nature immunology*  
305 **18**, 412-421, doi:10.1038/ni.3683 (2017).
- 306 22 Sen, D. R. *et al.* The epigenetic landscape of T cell exhaustion. *Science* **354**,  
307 1165-1169, doi:10.1126/science.aae0491 (2016).
- 308 23 Im, S. J. *et al.* Defining CD8+ T cells that provide the proliferative burst after  
309 PD-1 therapy. *Nature* **537**, 417-421, doi:10.1038/nature19330 (2016).
- 310 24 Chen, L. & Flies, D. B. Molecular mechanisms of T cell co-stimulation and co-  
311 inhibition. *Nature reviews Immunology* **13**, 227-242, doi:10.1038/nri3405  
312 (2013).
- 313

314 **Figure Legends**315 **Figure 1. Multiple co-inhibitory receptors are expressed as a module on CD4<sup>+</sup> and**  
316 **CD8<sup>+</sup> T cells**

317 **a)** CD4<sup>+</sup> and CD8<sup>+</sup> tumor-infiltrating lymphocytes (TILs) were harvested from WT mice  
318 bearing B16F10 melanoma tumors. Top panels, co-expression analysis of co-inhibitory  
319 and co-stimulatory receptor mRNA expression as determined by single-cell RNA-seq for  
320 316 CD4<sup>+</sup> and 588 CD8<sup>+</sup> TILs. Bottom panels, protein expression by CyTOF for 23,656  
321 CD4<sup>+</sup> and 36,486 CD8<sup>+</sup> TILs. Spearman correlation, followed by dendrogram ordering of  
322 the matrix using Euclidian distance is shown. Data are from biologically independent  
323 experiments. **b)** TILs from WT mice bearing B16F10 melanoma were analyzed using  
324 CyTOF with a custom panel of antibodies against co-inhibitory and co-stimulatory cell  
325 surface receptors<sup>2,24</sup> (**Supplementary Information Table 1**). Data were analyzed using  
326 vi-SNE. Polygons indicating clusters 1, 2 (in CD8<sup>+</sup> T cells), 3 and 4 (in CD4<sup>+</sup> T cells) are  
327 shown. Individual panels show expression of the indicated markers. **c)** Naïve T cells from  
328 either wild type (WT) or IL-27ra deficient (IL27ra KO) mice were stimulated with anti-  
329 CD3/CD28 in the presence or absence of IL-27. Indicated co-inhibitory receptors  
330 expression was examined by real-time PCR (qPCR) at 96hr (CD4) and 72hr (CD8). Data  
331 are from biologically independent animals. mean  $\pm$  s.e.m is shown. **d)** vi-SNE plot  
332 showing WT (red) and IL27ra KO (blue) cells. **e)** ScRNA-seq of TILs from mice bearing  
333 B16F10 melanoma. Data were analyzed using t-SNE. Polygons indicating cluster 4 (in  
334 CD4<sup>+</sup> T cells, orange) and cluster 5 (in CD8<sup>+</sup> T cells, blue) are shown. Individual panels  
335 show expression of the indicated markers. Bar graphs show the mean signal intensity for  
336 indicated co-inhibitory receptors from WT (CD4<sup>+</sup> (n=849); CD8<sup>+</sup> (n=1752)) and IL27ra

337 KO (CD4<sup>+</sup> (n=628); CD8<sup>+</sup> (n=541)) TILs for CyTOF (d) or WT (CD4<sup>+</sup> (n=707); CD8<sup>+</sup>  
 338 (n=825)) and IL27ra KO (CD4<sup>+</sup> (n=376); CD8<sup>+</sup> (n=394)) TILs for ScRNA-seq (e). Error  
 339 bars indicate s.e.m. and \*p < 0.05, \*\*p < 0.01, \*\*\*p < 0.001; two-sided t-test.

340

341 **Figure 2. The IL-27-induced gene program overlaps with multiple signatures of T**  
 342 **cell dysfunction and tolerance**

343 **a)** Panels I-VI, tSNE plots of the 588 CD8<sup>+</sup> single-cell TILs (dots) harvested from WT  
 344 mice bearing B16F10 melanoma. Cells are colored in each panel by their signature score  
 345 that reflects the relative average expression of the genes in the overlap of the IL-27-  
 346 induced gene program with the signatures for each of the indicated states of T cell non-  
 347 responsiveness. Panel VI is a projection of a signature of the differentially expressed  
 348 genes between CD8<sup>+</sup> TILs from WT and IL27ra KO mice bearing B16 melanoma  
 349 (**Methods**). The contour marks the region of highly scored cells based on cells with  
 350 signature scores above the mean. **b)** Graphical representation of the overlap of 57 IL-27-  
 351 induced cell surface receptors or cytokine genes with genes expressed in different states  
 352 of T cell non-responsiveness. The width of the gray bars reflects the extent of overlap  
 353 across states. Significance of the overlap genes between the IL-27 induced and each  
 354 state of T cell non-responsiveness state were calculated using Wilcox GST and  
 355 camera. **c)** Graphical representation of the selected overlap genes between the cancer  
 356 exhaustion and the chronic viral exhaustion signatures. The shaded background reflects  
 357 the ranking based on the extent of overlap with the T cell states depicted. **d)** WT (n=8)  
 358 mice and Procr<sup>d/d</sup> (n=7) or **e)** WT (n=5) and Pdpn cKO (n=5) mice were implanted with  
 359 B16F10 melanoma. Data are from 3 biologically independent experiments. Mean tumor



360 size  $\pm$  s.e.m is shown. \*\*\*\*P<0.0001, repeated measures ANOVA, Sidak's multiple  
 361 comparisons test. e and h) Summary of flow cytometry data for cytokine production in  
 362 the indicated CD8<sup>+</sup> TILs. f and i) Left panels, representative flow cytometry data for  
 363 Tim-3 and PD-1 expression on the indicated CD8<sup>+</sup> TILs. Right panels, summary data. e-i)  
 364 \*p < 0.05; \*\*p < 0.01; \*\*\*p < 0.001, two-sided t-test.

365

366 **Figure 3. Prdm1 and c-Maf individually regulate co-inhibitory receptors on T cells**

367 a) Summary data of co-inhibitory receptor expression on CD8<sup>+</sup> TILs from WT and  
 368 Prdm1 cKO mice bearing B16F10 melanoma. Data are from biologically independent  
 369 animals. mean  $\pm$  s.e.m is shown. \*p<0.05, \*\*\*p<0.001, two-sided t-test. b) WT (n=5) and  
 370 Prdm1 cKO (n=5) mice were implanted with B16F10 melanoma. Mean tumor size  $\pm$   
 371 s.e.m. is shown. Data are from 3 biologically independent experiments. c) Left panel,  
 372 gene expression in CD8<sup>+</sup> TILs from WT and Prdm1 cKO mice bearing B16F10  
 373 melanoma was analyzed by n-counter code-set (**Supplementary Information Table 3**).  
 374 Differentially expressed genes are shown as a heatmap. Right panel, expression of c-Maf  
 375 in CD8<sup>+</sup> TILs from WT and Prdm1 cKO mice as determined by qPCR. Data are from  
 376 biologically independent animals. mean  $\pm$  s.e.m is shown. p = 0.03, two-sided t-test. d)  
 377 Summary data of co-inhibitory receptor expression on CD8<sup>+</sup> TILs from WT and c-Maf  
 378 cKO. Data are from biologically independent animals. mean  $\pm$  s.e.m is shown. \*p < 0.05,  
 379 two-sided t-test. e) Frequency of co-inhibitory receptor expression of Prdm1 cKO (gray  
 380 bar) and c-Maf cKO (open bar) CD8<sup>+</sup> TILs relative to WT (filled bar). Data are from 3a  
 381 and 3d, mean  $\pm$  s.e.m is shown. f) Left panel, WT (n=8) and c-Maf cKO (n=5) mice were  
 382 implanted with B16F10 melanoma. Mean tumor size  $\pm$  s.e.m is shown. Data are from two

383 biologically independent experiments. Right panel, expression of Prdm1 in CD8<sup>+</sup> TILs  
 384 from WT and c-Maf cKO mice as determined by qPCR.

385

386 **Figure 4. Prdm1 and c-Maf together regulate a co-inhibitory gene module that**  
 387 **determines anti-tumor immunity**

388 **a)** Network model based on coupling RNAseq gene expression data of naïve CD8<sup>+</sup> T  
 389 cells from Prdm1 cKO or c-Maf cKO mice stimulated in the presence of IL-27 and  
 390 Prdm1 and c-Maf ChIPseq data. Up-regulated genes (green arrows), down-regulated  
 391 genes (red arrows), and c-Maf or Prdm1 binding events (gray arrows) are shown. **b)**  
 392 Summary data of indicated co-inhibitory receptors expression on CD8<sup>+</sup> TILs from WT  
 393 and Prdm1/c-Maf cDKO bearing B16F10 melanoma. Data are from biologically  
 394 independent animals. mean  $\pm$  s.e.m is shown. \*\*p < 0.01; \*\*\*p < 0.001, two-sided t-test.

395 **c)** WT (n=15) and cDKO (n=8) mice were implanted with B16F10 melanoma. Data  
 396 shown are from 3 biologically independent experiments. **d)** CD4<sup>+</sup> or CD8<sup>+</sup> T cells sorted  
 397 from cDKO mice or littermate controls were transferred into Rag1 KO mice at a 2:1  
 398 CD4:CD8 ratio followed by subcutaneous injection of B16-OVA (n=5, each condition).

399 Data are representative of 3 biologically independent experiments. c-d) Mean tumor size  
 400  $\pm$  s.e.m is shown. \*P<0.05, \*\*P<0.01, \*\*\*\*P<0.0001, repeated measures ANOVA,

401 Sidak's multiple comparisons test. **e-f)** T cells were harvested from Rag1 KO mice that  
 402 received an adoptive transfer of CD4<sup>+</sup> and CD8<sup>+</sup> T cells from WT or cDKO mice (2:1  
 403 CD4:CD8 ratio) followed by subcutaneous injection of MC38-OVA (**Extended Data**

404 **Fig. 8e**). **e)** The frequency of IFN- $\gamma$  and TNF- $\alpha$  CD8<sup>+</sup> TILs after OVA-peptide  
 405 stimulation, **f)** the frequency and expression of Ki67<sup>+</sup> cells on splenocytes (upper panel),

406 and the frequency of IFN- $\gamma$  and TNF- $\alpha$  CD8<sup>+</sup> splenocytes (lower panel) after OVA-  
407 peptide stimulation. mean  $\pm$  s.e.m is shown. Data are from biologically independent  
408 animals. \*P<0.05, \*\*P<0.01, two-sided t-test. **g)** 940 differentially expressed genes  
409 between CD8<sup>+</sup> TILs from WT and cDKO bearing B16F10 melanoma. (adj. P. value<0.05,  
410 likelihood ratio test and FDR correction) (top panel) and their corresponding expression  
411 pattern in PD-1<sup>+</sup>Tim-3<sup>+</sup> CD8<sup>+</sup>, PD-1<sup>+</sup>Tim-3<sup>-</sup> CD8<sup>+</sup>, and PD-1<sup>-</sup>Tim-3<sup>-</sup> CD8<sup>+</sup> TILs.

412

413

**414 Methods****415 Mice**

416 C57BL/6 wild-type (WT), IL27ra KO, and Prdm1 fl/fl mice were obtained from the  
417 Jackson Laboratory (Bar Harbor, ME). c-Maf fl/fl, Pdpn fl/fl mice and Procr delta/delta  
418 mice were previously described<sup>13,15,26</sup>. Pdpn fl/fl mice were initially obtained from  
419 Christopher Buckley (University of Birmingham, Birmingham, UK) and crossed to  
420 CD4Cre mice to obtain conditional deletion in T cell. CD4Cre mice were purchased from  
421 Taconic (Hudson, NY). Prdm1 fl/fl and c-Maf fl/fl mice were crossed to CD4Cre mice to  
422 generate doubly deficient T cell conditional knockout mice. All experiments were  
423 performed in accordance to the guidelines outlined by the Harvard Medical Area  
424 Standing Committee on Animals (Boston, MA).

425

**426 Tumor Experiments**

427  $5 \times 10^5$  B16F10 melanoma cells (ATCC) were implanted into the right flank of C57BL/6  
428 mice. Tumor size was measured in two dimensions using a caliper. TILs were isolated by  
429 dissociating tumor tissue in the presence of 2.5 mg/ml collagenase D for 20 min before  
430 centrifugation on a discontinuous Percoll gradient (GE Healthcare). Isolated cells were  
431 then used in various assays of T cell function. For antigen specific analysis, we applied  
432 adoptive transfer tumor experiments using T cells from Prdm1/c-Maf cDKO mice, CD4<sup>+</sup>  
433 or CD8<sup>+</sup> T cells sorted from cDKO mice or littermate controls were transferred into Rag1  
434 KO mice at a 2:1 ratio (CD4: 1 million/mouse and CD8: 0.5 million/mouse) 2 days  
435 before subcutaneous injection of B16-OVA or MC38-OVA tumor. B16-Ova was kind gift  
436 from Kai Wucherpfennig (Dana-Farber Cancer Institute, Boston, MA) and MC38-Ova

437 was kind gift from Mark Smyth (QIMR Berghofer, Queensland Institute of Medical  
438 Research, Brisbane Australia). For adoptive transfer tumor experiments using T cells  
439 from Procr<sup>d/d</sup> mice, CD4<sup>+</sup> T cells from WT and CD8<sup>+</sup> T cells from WT or Procr<sup>d/d</sup> mice  
440 were isolated by cell sorting (BD FACS Aria) and transferred into Rag deficient recipient  
441 mice at a 2:1 ratio (WT CD4<sup>+</sup>: 1 million/mouse and WT or Procr<sup>d/d</sup> CD8<sup>+</sup>: 0.5  
442 million/mouse) 2 days before tumor implant. Although we did not blinding or  
443 randomization, at least 5 animals of target gene knock out and control mice were used to  
444 adequately power biological validation experiments throughout the article. All mice used  
445 are C57BL/6 background, both male and female, 6-12 weeks of age, 15-25g. Each  
446 experiment was performed using age, sex matched controls (**Supplementary**  
447 **Information Table 5**).

448

449 **CyTOF**

450 Antibodies were labeled using MaxPar® Metal Labeling Kits (DVS) by The Longwood  
451 Medical Area CyTOF Antibody Resource and Core. In some experiments, TILs were  
452 enriched using Dynabeads FlowComp Mouse Pan T (CD90.2) Kit (Invitrogen). Cells  
453 were washed and resuspended in CyTOF PBS (PBS + 0.05% sodium azide + 0.5% BSA)  
454 and stained viability marker Rhodium (DVS) following the cocktail of antibodies against  
455 cell-surface molecules for 30 min. Cells were washed again and resuspended in CyTOF  
456 PBS with 4% paraformaldehyde. After 10 min fixation, cells were washed and barcoded  
457 with Cell-ID intercalators (DVS). Before analysis, cells were resuspended in water with  
458 beads and loaded to the CyTOF® Mass Cytometer (DVS). CyTOF data were recorded in  
459 dual-count according to Fluidigm's recommended settings that calibrated on the fly,

460 combining pulse-count and intensity information. Data obtained as mass peaks for the  
461 channels are processed according to cell event selection criteria. These criteria include  
462 cell viability selection (Pt195), single-cell selection (Intercalator-Ir), and barcoding  
463 selection (Pt194 and Pt198) to identify single-cell events from WT TILs and KO TILs for  
464 further analysis.

465 To obtain clusters of cells similar in their protein expression patterns, cells were  
466 clustered using k-means algorithm. Optimal cluster number was estimated using the  
467 within groups sum of squared error (SSE) plot followed by gap statistics with  
468 bootstrapping and first SE max method. These methods suggested 9 clusters as optimal in  
469 the multidimensional space. Applying k-means clustering with (k=9) on our CyTOF data,  
470 resulted in clear distinction between cluster 1 and 2 of the CD8<sup>+</sup> TILs and cluster 3 and 4  
471 of the CD4<sup>+</sup> TILs. This separation could be further visualized by two-dimensional non-  
472 linear embedding of the protein expression profiles using t-stochastic neighborhood  
473 embedding (t-SNE<sup>4</sup>). The t-SNE plot can then be overlaid by k-means clustering results  
474 to reflect a non-biased approach to the clusters or with intensity of the different markers.

475

#### 476 **Flow Cytometry**

477 Single cell suspensions were stained with antibodies against CD4 (RM4-5), CD8 (53-  
478 6.7), PD-1 (RMP1-30), Lag-3 (C9B7W), TIGIT (GIGD7), and Tim-3 (5D12), Procr  
479 (eBio1560), and Pdpn (8.1.1.) were obtained from BioLegend (San Diego, CA). Fixable  
480 viability dye eF506 (eBioscience) was used to exclude dead cells. For intra-cytoplasmic  
481 cytokine staining, cells were stimulated with (PMA) (50ng/ml, Sigma-Aldrich, MO),  
482 ionomycin (1µg/ml, Sigma-Aldrich, MO). Permeabilized cells were then stained with

483 antibodies against IL-2, TNF- $\alpha$ , IFN- $\gamma$  or IL-10. All data were collected on a BD LSR II  
484 (BD Biosciences) and analyzed with FlowJo software (Tree Star).

485

#### 486 ***In vitro* T cell differentiation**

487 CD4<sup>+</sup> and CD8<sup>+</sup> T cells were purified from spleen and lymph nodes using anti-CD4  
488 microbeads and anti-CD8a microbeads (Miltenyi Biotech) then stained in PBS with 0.5%  
489 BSA for 15 min on ice with anti-CD4, anti-CD8, anti-CD62L, and anti-CD44 antibodies  
490 (all from Biolegend, CA). Naïve CD4<sup>+</sup> or CD8<sup>+</sup> CD62L<sup>high</sup>CD44<sup>low</sup> T cells were sorted  
491 using the BD FACSAria cell sorter. Sorted cells were activated with plate bound anti-  
492 CD3 (2 $\mu$ g/ml for CD4 and 1 $\mu$ g/ml for CD8) and anti-CD28 (2 $\mu$ g/ml) in the presence of  
493 rmIL-27 (25ng/ml) (eBioscience). Cells were harvested at various time points for RNA,  
494 intracellular cytokine staining, and flow cytometry.

495

#### 496 **Real-time PCR**

497 Total RNA was extracted using RNeasy columns (Qiagen). Reverse transcription of  
498 mRNA was performed in a thermal cycler (Bio-Rad) using iScript™ cDNA Synthesis Kit  
499 (Bio-Rad). Real-time PCR was performed in the Vii7™ Real-Time PCR system (Applied  
500 Biosystems) using the primers for Taqman gene expression (Applied Biosystems). Data  
501 was normalized to the expression of ACTB.

502

#### 503 **Nanostring RNA analysis**

504 **Expression profiling of TILs.** We analyzed gene expression in CD8<sup>+</sup> TILs from Prdm1  
505 or c-Maf cKO mice bearing B16F10 melanoma collected on day 14 after tumor

506 implantation, using a custom nanostring code-set of 397 genes representing both the IL-  
507 27-driven gene signature (245 genes) and the dysfunctional CD8<sup>+</sup> TIL gene signature  
508 (245 genes) (**Supplementary Information Table 3**). Expression values were normalized  
509 by first adjusting each sample based on its relative value to all samples. This was  
510 followed by subtracting the calculated background (mean.2sd) from each sample with  
511 additional normalization by housekeeping geometric mean, where housekeeping genes  
512 were defined as: Hprt, Gapdh, Actin and Tubb5. Differentially expressed genes were  
513 defined using the function that fits multiple linear models from the Bioconductor package  
514 limma in R<sup>27</sup> with p-value<0.05.

515

#### 516 **Microarray processing and analysis**

517 Naïve CD4<sup>+</sup> and CD8<sup>+</sup> T cells were isolated from WT or IL27ra KO mice, and  
518 differentiated *in vitro* with or without IL-27. Cells were collected at 72 hours for CD8<sup>+</sup>  
519 and 96 hours for CD4<sup>+</sup> and Affymetrix GeneChip Mouse Genome 430 2.0 Arrays were  
520 used to measure the resulting mRNA levels at these time points. Individual .CEL files  
521 were RMA normalized and merged to an expression matrix using the  
522 ExpressionFileCreator of GenePattern with default parameters<sup>28</sup>. Gene-specific intensities  
523 were then computed by taking for each gene *j* and sample *i* the maximal probe value  
524 observed for that gene. Samples were then transferred to log-space by taking  
525  $\log_2(\text{intensity})$ .

526 Differentially expressed genes were annotated as genes with FDR-corrected  
527 ANOVA <0.05 computed between the CD4 with or without IL-27 stimulation (CD4<sup>+</sup>  
528 IL27 and Th0) subpopulations (1,202 genes). 468 genes were differentially expressed



529 between WT CD8<sup>+</sup> T cells stimulated in the presence or absence of IL-27 (p-value<0.05).  
530 234 genes were shared between these two differentially expressed gene lists (p-value =  
531  $2.25 \times 10^{-157}$ , hypergeometric test, background=16,618 (union of genes expressed)). A list  
532 of 972 cell surface/cytokines genes of interest that include: cytokines, adhesion,  
533 aggregation, chemotaxis and other cell surface molecules (**Supplementary Information**  
534 **Table 4**) composed using GO annotation in Biomart was used to generate the gene subset  
535 in **Fig. 2b** and **c**.

536

537

### 538 **RNAseq gene expression profiling of tumor infiltrating cells**

539 Tumor infiltrating CD8<sup>+</sup> T cells were isolated from WT, IL27ra KO, Prdm1 cKO, c-Maf  
540 cKO, and Prdm1/c-Maf cDKO tumor bearing mice via FACS sorting on a FACSAria (BD  
541 Biosciences). Tumor infiltrating CD8<sup>+</sup> T cells were processed using an adaptation of the  
542 SMART-Seq 2 protocol<sup>29</sup>, using 5uL of lysate from bulk CD8<sup>+</sup> T cells as the input for  
543 each sample during RNA cleanup via SPRI beads (~2,000 cells lysed on average in RLT).

544 RNA-seq reads were aligned using Tophat<sup>30</sup> (mm9) and RSEM-based  
545 quantification<sup>31</sup> using known transcripts (mm9), followed by further processing using the  
546 Bioconductor package DESeq in R<sup>32</sup>. The data was normalized using TMM  
547 normalization. The TMM method estimates scale factors between samples that can be  
548 incorporated into currently used statistical methods for DE analysis. Post-processing and  
549 statistical analysis was carried out in R<sup>31</sup>. Differentially expressed genes were defined  
550 using the differential expression pipeline on the raw counts with a single call to the

551 function DESeq (adjusted p value<0.1). Heatmap figures were generated using pheatmap  
552 package<sup>33</sup>.

553

#### 554 **Single-cell RNA-seq**

555 CD4<sup>+</sup> and CD8<sup>+</sup> TILs from WT or IL27ra KO mice bearing B16 melanomas were sorted  
556 into 96-well plates with 5 µl lysis buffer comprised of Buffer TCL (Qiagen) plus 1% 2-  
557 mercaptoethanol (Sigma). Plates were then spun down for one minute at 3000rpm and  
558 immediately frozen at -80°C. Cells were thawed and RNA was isolated with 2.2x  
559 RNAClean SPRI beads (Beckman Coulter Genomics) without final elution<sup>34</sup>. The beads  
560 were then air-dried and processed immediately for cDNA synthesis. Samples were then  
561 processed using the Smart-seq2 protocol<sup>35</sup>, with minor modifications applied to the  
562 reverse transcription (RT) step (MSK and AR., in preparation). This was followed by  
563 making a 25µl reaction mix for each PCR and performing 21 cycles for cDNA  
564 amplification. Then 0.25 ng cDNA from each cell and ¼ of the standard Illumina  
565 NexteraXT reaction volume were used in both the tagmentation and final PCR  
566 amplification steps. Finally, libraries were pooled and sequenced (50 x 25 paired-end  
567 reads) using a single kit on the NextSeq500 5 instrument. All CD4<sup>+</sup> TILs (WT and IL27ra  
568 KO) single-cell RNA-seq data was generated as part of this study. CD8<sup>+</sup> TILs single-cell  
569 data includes WT CD8<sup>+</sup> TILs data from<sup>3</sup> and WT and IL27ra KO CD8<sup>+</sup> single-cell data  
570 generated as part of this study.

571

#### 572 **Single-cell RNA-seq data preprocessing and expression**

573 Initial preprocessing was performed as described in<sup>3</sup>. Briefly, paired reads were mapped  
574 to mouse annotation mm10 using Bowtie<sup>36</sup> (allowing a maximum of one mismatch in  
575 seed alignment, and suppressing reads that had more than 10 valid alignments) and TPMs  
576 were computed using RSEM<sup>31</sup>, and  $\log_2(\text{TPM}+1)$  values were used for subsequent  
577 analyses.

578 Next, we filtered out low quality cells and cell doublets, maintaining for  
579 subsequent analysis the cells that had (1) 1,000-4,000 detected genes (defined by at least  
580 one mapped read), (2) at least 200,000 reads mapped to the transcriptome, and (3) at least  
581 50% of the reads mapped to the transcriptome, ending with a total of 707 CD4<sup>+</sup> and 825  
582 CD8<sup>+</sup> WT TILs and 376 CD4<sup>+</sup> and 394 CD8<sup>+</sup> IL27ra KO TILs. We restricted the genes  
583 considered in subsequent analyses to be the genes expressed at  $\log_2(\text{TPM}+1) \geq 2$  in at  
584 least twenty percent of the cells.

585 After removal of low quality cells the data was normalized using quantile  
586 normalization followed by PCA analysis. PCs 1-10 were chosen for subsequent analysis  
587 due to a drop in the proportion of variance explained following PC10. We used tSNE<sup>4</sup> to  
588 visualize single-cells in a two-dimensional non-linear embedding.

589

### 590 **Single-cell RNA-seq clustering and differential expression analysis**

591 For the coupled dataset of WT and IL27ra KO TILs we followed the analysis described in  
592 <sup>37</sup>. We performed batch correction using ComBat<sup>38</sup> and the batch-corrected expression  
593 matrix was then reduced using PCA, PCs 1-13 were chosen for subsequent analysis due  
594 to a drop in the proportion of variance explained following PC13. Next, we cluster the  
595 cells based on their PC scores using the Louvain-Jaccard method using 40 nearest

596 neighbors, and the 13 PCs<sup>25,39</sup>; 11 clusters were detected. We then compared the  
597 composition of each cluster in terms of total number and percentage of WT and IL27ra  
598 KO cells and found cluster 5 to be enriched for WT CD8 TILs cells (p-value= 0.0357,  
599 one sample t-test, **Extended Data Fig. 3c,d**). Projecting the IL-27 co-inhibitory gene  
600 module onto the single-cell RNA-seq data highlighted clusters 4 and 5 (CD4 and CD8  
601 respectively) (**Extended Data Fig. 3e**), further showing that in addition to the decrease in  
602 the expression of the co-inhibitory receptors: PD-1, Tim-3, Lag-3 and TIGIT (**Fig. 1e**), a  
603 significant decrease in the total IL-27 co-inhibitory gene module signature score is  
604 observed with lack of IL-27 signaling (p-value=0.01, t-test, **Extended Data Fig. 3f**).  
605 Last, we searched for differentially expressed genes between clusters 4/5 and the  
606 rest of the clusters using a nonparametric binomial test<sup>37</sup>.

607

### 608 **Signature analysis of other states of T cell non-responsiveness**

609 Given that orthogonal approaches were used to generate the various signatures, we first  
610 addressed the robustness of each signature prior to the comparative analysis. First, to  
611 address some of the concerns regarding the definition of these signatures we sub-sampled  
612 the genes in each of the signatures and observed the resulting changes by projection on  
613 the single-cell data. These changes were quantified by randomly selecting decreasing  
614 subsets of genes from each signature (100%, 90% ... 30%) and calculating the average  
615 silhouette width of the cells that scored high for the different generated signatures, based  
616 on Euclidian distance between the principal component values used to generate the tSNE  
617 plot. This analysis shows that the signatures are relatively resilient to this procedure up  
618 to 60% of the original signature (**Extended Data Fig. 4e**).

619           Second, we calculated a signature p-value per cell. The p-value is calculated by  
620 generating random sets of signatures that are composed of genes with a similar average  
621 and variance expression levels as the original signature. This was followed by comparing  
622 the generated scores to the score obtained from the original signature. Cells that had a  
623 statistically significant score (adjusted p-value<0.05) were marked by '+' (**Extended**  
624 **Data Fig. 4f**).

625           For viral exhaustion: Microarray dataset<sup>10</sup> was downloaded, followed by RMA. A  
626 signature of viral exhaustion was defined as the genes that are differentially expressed  
627 between chronic and acute viral infection on day 15 and day 30. Genes were ranked  
628 based on a *t*-test statistic and fold change, each gene rank was then adjusted for multiple  
629 hypotheses testing using false discovery rate (FDR). A threshold of fold change>1.1 and  
630 FDR<0.2 was applied.

631           For antigen-specific tolerance: Data<sup>11</sup> were downloaded. Two groups were  
632 defined, group 1 that includes the PBS and 0.008 µg treated samples (treatment number  
633 1) versus group 2 - 80 µg (treatment number 5 and 6). After Log2 transformation and  
634 quantile normalization, the Limma package was used to estimate the fold changes and  
635 standard errors by fitting a linear model for each gene for the assessment of differential  
636 expression. Genes with p value < 0.05 were selected: 1,845 genes were upregulated of  
637 which 88 were defined as cytokine and cell surface molecules<sup>27,40,41</sup>.

638           For antigen non-specific tolerance: Data<sup>12</sup> was downloaded. Robust Multi-array  
639 Average (RMA) and quantile normalization were applied for background correction and  
640 normalization using the ExpressionFileCreator module of GenePatterns. Differentially  
641 expressed genes were defined using signal-to-noise ratio (SNR), following FDR

642 correction. Differentially expressed genes were identified as genes having a FDR<0.2  
643 between mRNA expression profiles of naïve CD4<sup>+</sup> or CD4<sup>+</sup> GFP/IL-10<sup>+</sup> T cells isolated  
644 from the spleen or cLNs of B6NOD.F1<sup>IL10:GFP</sup> mice following nasal treatment with anti-  
645 CD3 which attenuates the of progressive phase of EAE.

646 For cancer: Data<sup>3</sup> was obtained. Briefly, mRNA samples from CD8<sup>+</sup>Tim-3<sup>-</sup>PD-1<sup>-</sup>  
647 (DN) TILs, CD8<sup>+</sup>Tim-3<sup>-</sup>PD-1<sup>+</sup>(SP), and CD8<sup>+</sup>Tim-3<sup>+</sup>PD-1<sup>+</sup> (DP) TILs were measured  
648 using Affimetrix GeneChip Mouse Genome 430 2.0 Arrays, expression values were RMA  
649 normalized, corrected for batch effects using ComBat<sup>38</sup> and gene-specific intensities were  
650 then computed by using the maximal prob intensity per gene, values were transferred to  
651 log-space by taking log<sub>2</sub>(intensity). Differentially expressed genes were defined as genes  
652 with either an FDR-corrected t-test p-value smaller or equal to 0.2 computed between the  
653 DN and DP subpopulations and a fold-change of at least 1.5 between the two  
654 subpopulations.

655 The IL-27 co-inhibitory gene module was defined as a union of the overlap  
656 between the IL-27-driven gene program (1,201 genes see **Methods**: Microarray  
657 processing and analysis) and each of the four different states of T cell non-responsiveness  
658 mentioned above (272 genes, **Supplementary Information Table 2**).

659 For IL27ra KO signature: mRNA samples from FACS sorted CD8<sup>+</sup> TILs from  
660 WT and IL27ra KO mice bearing B16 melanomas were measured an adaptation of the  
661 SMART-Seq 2 protocol<sup>29</sup> (see **Method: RNA expression profiling of tumor infiltrating**  
662 **cells**). Differentially expressed genes were defined as genes with either an FDR-corrected  
663 t-test p-value smaller or equal to 0.2 computed between the WT and IL27ra KO and a  
664 fold-change of at least 1.5 between the two subpopulations. IL27ra KO signature was

665 defined as 929 differentially expressed genes in IL27ra KO CD8<sup>+</sup> TILs compared to WT  
666 CD8<sup>+</sup> TILs.

667

### 668 **Single-cell gene signature computation**

669 As an initial step, the data was scaled (z-score across each gene) to remove bias towards  
670 highly expressed genes. Given a gene signature (list of genes), a cell-specific signature  
671 score was computed by first sorting the normalized scaled gene expression values for  
672 each cell followed by summing up the indices (ranks) of the signature genes. For gene-  
673 signatures consisting of an upregulated and downregulated set of genes, two ranking  
674 scores were obtained separately, and the down-regulated associated signature score was  
675 subtracted from the up-regulated generated signature score. A contour plot was added on  
676 top of the tSNE space, which takes into account only those cells that have a signature  
677 score above the mean to further emphasis the region of highly scored cells.

678

### 679 **Network construction**

680 Networks were generated using Cytoscape version 3.2.1<sup>42</sup>. The network model is based  
681 on coupling *in vitro* RNAseq gene expression data of naïve CD8<sup>+</sup> T cells from KO  
682 (Prdm1 or c-Maf) and WT controls stimulated in the presence of IL-27 and previously  
683 published ChIP-seq data for c-Maf and predicted Prdm1 binding sites by motif scan.  
684 More specifically, differentially expressed genes between WT control and KO were  
685 defined using the function that fits multiple linear models from the Bioconductor package  
686 limma in R<sup>27</sup> with FDR<0.05. We used published c-Maf ChIP-seq data<sup>19</sup> and Prdm1  
687 ChIP-seq data<sup>16</sup>. In addition, potential Prdm1 binding sites were detected using FIMO

688 (MEME suite - <http://meme-suite.org/doc/fimo.html>). Association to gene promoters was  
 689 based on the following thresholds (upstream=5000, downstream=500 of TSS) and the  
 690 overlap with the co-inhibitory module was found to be significant (p-value= 0.009 hyper  
 691 geometric, background of 20,000 genes). In the network presentation, we visualize all the  
 692 genes that are part of the IL-27 inhibitory module (**Extended Data Fig. 6e** and **Fig. 4a**).

693

#### 694 **Data availability**

695 Sequence data that support the findings of this study have been deposited in GEO  
 696 with the accession codes XXX

697

#### 698 **References for Method and Extended Data**

- 699 25 Blondel, V. D., Guillaume, J. L., Lambiotte, R. & Lefebvre, E. Fast unfolding of  
 700 communities in large networks. *J. Stat. Mech.*, P10008 (2008).
- 701 26 Wende, H. *et al.* The transcription factor c-Maf controls touch receptor  
 702 development and function. *Science* **335**, 1373-1376,  
 703 doi:10.1126/science.1214314 (2012).
- 704 27 Smyth, G. K. Linear models and empirical bayes methods for assessing  
 705 differential expression in microarray experiments. *Statistical applications in*  
 706 *genetics and molecular biology* **3**, Article3, doi:10.2202/1544-6115.1027  
 707 (2004).
- 708 28 Reich, M. *et al.* GenePattern 2.0. *Nat Genet* **38**, 500-501, doi:10.1038/ng0506-  
 709 500 (2006).
- 710 29 Tirosh, I. *et al.* Dissecting the multicellular ecosystem of metastatic  
 711 melanoma by single-cell RNA-seq. *Science* **352**, 189-196,  
 712 doi:10.1126/science.aad0501 (2016).
- 713 30 Trapnell, C., Pachter, L. & Salzberg, S. L. TopHat: discovering splice junctions  
 714 with RNA-Seq. *Bioinformatics* **25**, 1105-1111,  
 715 doi:10.1093/bioinformatics/btp120 (2009).
- 716 31 Li, B. & Dewey, C. N. RSEM: accurate transcript quantification from RNA-Seq  
 717 data with or without a reference genome. *BMC Bioinformatics* **12**, 323,  
 718 doi:10.1186/1471-2105-12-323 (2011).
- 719 32 Anders, S. & Huber, W. Differential expression analysis for sequence count  
 720 data. *Genome Biol* **11**, R106, doi:10.1186/gb-2010-11-10-r106 (2010).
- 721 33 Kolde, R. (R package version 1.0.2, 2015).



- 722 34 Shalek, A. K. *et al.* Single-cell transcriptomics reveals bimodality in  
 723 expression and splicing in immune cells. *Nature* **498**, 236-240,  
 724 doi:10.1038/nature12172 (2013).
- 725 35 Picelli, S. *et al.* Full-length RNA-seq from single cells using Smart-seq2. *Nat*  
 726 *Protoc* **9**, 171-181, doi:10.1038/nprot.2014.006 (2014).
- 727 36 Langmead, B., Trapnell, C., Pop, M. & Salzberg, S. L. Ultrafast and memory-  
 728 efficient alignment of short DNA sequences to the human genome. *Genome*  
 729 *Biol* **10**, R25, doi:10.1186/gb-2009-10-3-r25 (2009).
- 730 37 Shekhar, K. *et al.* Comprehensive Classification of Retinal Bipolar Neurons by  
 731 Single-Cell Transcriptomics. *Cell* **166**, 1308-1323 e1330,  
 732 doi:10.1016/j.cell.2016.07.054 (2016).
- 733 38 Johnson, W. E., Li, C. & Rabinovic, A. Adjusting batch effects in microarray  
 734 expression data using empirical Bayes methods. *Biostatistics* **8**, 118-127,  
 735 doi:10.1093/biostatistics/kxj037 (2007).
- 736 39 Levine, J. H. *et al.* Data-Driven Phenotypic Dissection of AML Reveals  
 737 Progenitor-like Cells that Correlate with Prognosis. *Cell* **162**, 184-197,  
 738 doi:10.1016/j.cell.2015.05.047 (2015).
- 739 40 Smyth, G. K. *Limma: linear models for microarray data.*, 397-420 (Springer,  
 740 2005).
- 741 41 Davis, S. & Meltzer, P. S. GEOquery: a bridge between the Gene Expression  
 742 Omnibus (GEO) and BioConductor. *Bioinformatics* **23**, 1846-1847,  
 743 doi:10.1093/bioinformatics/btm254 (2007).
- 744 42 Lopes, C. T. *et al.* Cytoscape Web: an interactive web-based network browser.  
 745 *Bioinformatics* **26**, 2347-2348, doi:10.1093/bioinformatics/btq430 (2010).
- 746
- 747 **Extended Data Figure Legends**

748

749 **Extended Data Figure 1. CyTOF analysis of co-inhibitory and co-stimulatory**  
 750 **receptor co-expression in TILs. a)** TILs were harvested from B16F10 melanoma tumor-  
 751 bearing WT and IL27ra KO mice from Fig. 1b and analyzed using CyTOF (5000 cells  
 752 from each). CyTOF data were analyzed using vi-SNE. Applying k-means clustering with  
 753 (k=9) on the CyTOF data resulted in clear distinction between clusters 1, 2, 3 and 4.  
 754 Polygons indicating clusters 1, 2 (in CD8<sup>+</sup> T cells), 3 and 4 (in CD4<sup>+</sup> T cells) are shown.  
 755 Individual panels show expression of the indicated markers. **b)** Pie charts show the  
 756 distribution of WT or IL27ra KO CD8<sup>+</sup> and CD4<sup>+</sup> TILs in clusters 1 and 2 (C1 and C2) of  
 757 CD8<sup>+</sup> TILs and clusters 3 and 4 (C3 and C4) of CD4<sup>+</sup> TILs as defined in **Fig. 1d. c)**

758 Independent data of WT and IL27ra KO TILs samples from that shown in **Fig. 1** (5000  
759 cells from each). Applying k-means clustering with (k=7) on the CyTOF data resulted in  
760 clear distinction between clusters 1, 2, 3 and 4. Polygons indicating clusters 1, 2 (in CD8<sup>+</sup>  
761 T cells), 3 and 4 (in CD4<sup>+</sup> T cells) are shown. **d)** vi-SNE plot highlighting the distribution  
762 of cells from WT (blue) and IL27ra KO (red) in CD8<sup>+</sup> TILs clusters 1 and 2 and CD4<sup>+</sup>  
763 TILs clusters 3 and 4. Pie charts show the distribution of WT or IL27ra KO CD8<sup>+</sup> and  
764 CD4<sup>+</sup> TILs in each cluster.

765

766 **Extended Data Figure 2. IL-27 induces multiple co-inhibitory receptors on CD4<sup>+</sup>**  
767 **and CD8<sup>+</sup> T cells.**

768 **a)** Naïve T cells from WT or IL27ra KO mice were stimulated *in vitro* with anti-  
769 CD3/CD28 in the presence or absence of IL-27. Expression of co-inhibitory receptors  
770 was determined by flow cytometry. Representative data of 3 biologically independent  
771 experiments are shown. **b)** Expression of PD-1, Tim-3, Lag-3, TIGIT, and IL-10 on CD8<sup>+</sup>  
772 TILs obtained from WT and IL27ra KO mice bearing B16F10 melanoma was determined  
773 by flow cytometry. Thy1.1-IL-10 reporter mice crossed with WT and IL27ra KO mice  
774 were used for IL-10 expression analysis. Representative data of 3 biologically  
775 independent experiments are shown.

776

777 **Extended Data Figure 3. Single-cell RNA-seq expression analysis of WT and IL27ra**  
778 **KO TILs.**

779 **a)** TILs were harvested from B16F10 melanoma tumor-bearing WT (707 and 825 for  
780 CD4<sup>+</sup> and CD8<sup>+</sup> respectively) and IL27ra KO (376 and 394 for CD4<sup>+</sup> and CD8<sup>+</sup>

781 respectively) mice as in **Fig. 1e**. t-SNE plot shows the presence of WT and IL27ra KO  
782 CD4<sup>+</sup> and CD8<sup>+</sup> TILs as indicated. **b**) Clustering using the Louvain-Jaccard method (40  
783 nearest neighbors and 13 principal components<sup>25</sup>). **c**) The composition of each cluster in  
784 terms of total number (c) and percentage (d) of WT (red) and IL27ra KO (blue) cells. P-  
785 values (\*p-value<0.05, \*\*p-value<0.01, \*\*\*p-value<0.001) were calculated using one  
786 sample t-test. **e**) Projection of the IL-27 co-inhibitory module signature on the single-cell  
787 RNA-seq data. The contour plot marks the region of highly expressing cells by taking  
788 into account only those cells that have an expression value above the mean. **f**) Violin and  
789 box plots displaying the distribution of the IL-27 co-inhibitory module signature score  
790 compared between WT (72 and 98 for CD4<sup>+</sup> and CD8<sup>+</sup> respectively) and IL27ra KO (85  
791 and 77 for CD4<sup>+</sup> and CD8<sup>+</sup> respectively) cells in clusters 4 and 5 (CD4<sup>+</sup> and CD8<sup>+</sup>  
792 respectively, \*p-value=0.01, one-sided t-test. The lower and upper hinges in the boxplot  
793 correspond to the first and third quartiles and the horizontal line corresponds to the  
794 median).

795

796 **Extended Data Figure 4. Overlap of the IL-27-induced gene program with**  
797 **signatures from four states of T cell impairment/tolerance/dysfunction.**

798 **a**) Pearson correlation between WT CD4<sup>+</sup> and CD8<sup>+</sup> T cells for the 1,201 genes that were  
799 differentially expressed between WT CD4<sup>+</sup> T cells stimulated in the presence or absence  
800 of IL-27 (FDR<0.05). **b**) Expression profile of 118 differentially expressed genes (from  
801 (a)) encoding cell surface receptors and cytokines are shown as a heatmap. **c**) The IL-27-  
802 induced gene program (1,201 genes) was compared to T cell signatures obtained from  
803 four states of T cell non-responsiveness. Number of overlapping genes between the IL-27

804 gene program and each signature is depicted. P values (\*\*p < 0.01) were determined  
805 by hypergeometric test: Nasal anti-CD3 –  $4.7 \times 10^{-21}$ , Cancer –  $1.2 \times 10^{-33}$ , antigen-specific  
806 tolerance –  $4 \times 10^{-14}$  and Viral exhaustion –  $1.7 \times 10^{-26}$ . **d)** p-value statistics for the  
807 significance of the overlap between the IL-27-induced gene program (1,201) and genes  
808 induced in other states of T cell non-responsiveness using wilcoxGST and camera. **e)**  
809 Gene signatures from (c) were sub-sampled and projected onto the CD8<sup>+</sup> single-cell TILs  
810 data. Changes were quantified by randomly selecting decreasing subsets of genes from  
811 each signature and calculating the average silhouette width of cells that scored high for  
812 the different generated signatures based on Euclidian distance between the principal  
813 component values used to generate the tSNE plot. The lower and upper hinges in the  
814 boxplot correspond to the first and third quartiles and the horizontal line corresponds to  
815 the median (**Methods**). **f)** Panels I-V, tSNE plots of the 588 CD8<sup>+</sup> single-cell TILs (dots)  
816 harvested from WT mice bearing B16F10 melanoma tumor. Cells are colored in each  
817 panel by their signature score. The score reflects the relative average expression of the  
818 genes in the overlap of the IL-27 gene signature with the signatures for each of the  
819 indicated states of T cell non-responsiveness. Panel VI is a projection of a signature of the  
820 differentially expressed genes between CD8<sup>+</sup> TILs from WT and IL27ra KO mice bearing  
821 B16 melanomas (**Methods**). The contour plot marks the region of highly scored cells by  
822 taking into account only those cells that have a signature score above the mean score.  
823 Cells that had a statistically significant score (adjusted p-value<0.05) were marked by ‘+’  
824 (**Methods**).  
825

**826 Extended Data Figure 5. Characterization of the role of Pdpn and Procr in CD8<sup>+</sup>****827 TILs**

828 **a)** Pdpn and Procr protein and mRNA expression was determined in T cells from WT and  
829 IL27ra KO stimulated with anti-CD3/CD28 in the presence or absence of IL-27. CD4<sup>+</sup>  
830 cells were analyzed at 96hr and CD8<sup>+</sup> cells at 72hr. Data are representative flow  
831 cytometry and qPCR data from biologically independent animals. mean  $\pm$  s.e.m is shown.

832 **b)** Representative flow cytometry data of 3 independent experiments showing Pdpn and  
833 Procr expression in PD-1<sup>+</sup>Tim-3<sup>+</sup> CD8<sup>+</sup> and PD-1<sup>-</sup>Tim-3<sup>-</sup> CD8<sup>+</sup> TILs obtained from WT  
834 and IL27ra KO mice bearing B16F10 melanoma. **c)** TILs from WT mice bearing B16F10  
835 melanoma were stimulated with PMA and Ionomycin. Cytokine production in Procr<sup>+</sup> or  
836 Procr<sup>-</sup> CD8<sup>+</sup> TILs is shown. Thy1.1-IL-10 reporter mice were used for IL-10 expression  
837 analysis. Data are from biologically independent animals. mean  $\pm$  s.e.m is shown. \*p <

838 0.05; \*\*p < 0.01, paired t-test. **d)** 5x10<sup>5</sup> CD8<sup>+</sup> T cells from wild type or Procr<sup>d/d</sup> mice  
839 were transferred along with 1x10<sup>6</sup> wild type CD4<sup>+</sup> T cells to Rag1 KO mice (N=5). On  
840 day 2, 5x10<sup>5</sup> B16F10 cells were implanted. Mean tumor size  $\pm$  s.e.m is shown. \*P<0.05,  
841 repeated measures ANOVA, Sidak's multiple comparisons test. **e)** TILs were obtained

842 from WT and Pdpn cKO mice bearing B16F10 melanoma and stained for the expression  
843 of IL-7Ra. Representative flow cytometry data from 3 independent animals. **f)** Summary  
844 data of IL-7Ra expression are from biologically independent animals. mean  $\pm$  s.e.m is  
845 shown. \*p < 0.05, one-sided t-test.

846

**847 Extended Data Figure 6. Prdm1 is a candidate regulator of the co-inhibitory**  
**848 module.**

849 **a)** Log2 fold change RNA levels between naïve CD4<sup>+</sup> or CD8<sup>+</sup> T cells simulated with or  
850 without IL-27. Data are from two independent experiments. Shown are transcription  
851 factors that are part of the IL-27 co-inhibitory module (Differentially expressed  
852 transcription factors were annotated as genes with FDR-corrected ANOVA <0.05). **b)**  
853 Transcription factors that are both in the IL-27 co-inhibitory module and are also  
854 overexpressed in clusters 4 and 5 in the single-cell data (clusters that were enriched for  
855 the IL-27 signature, **Extended data Fig. 3e,f**). Differentially expressed genes between  
856 clusters 4/5 and the rest of the clusters were determined using binomcount.test (binomial  
857 distribution, **Methods**). Log effect corresponds to log proportion of expressing cells and  
858 p-value is calculated by the probability of finding n or more cells positive for the gene in  
859 clusters 4/5 given the fraction in the rest of the clusters. **c)** tSNE plot of **Fig. 1e**. showing  
860 the expression of Prdm1 in WT (707 and 825 for CD4<sup>+</sup> and CD8<sup>+</sup>, respectively) and  
861 IL27ra KO (376 and 394 for CD4<sup>+</sup> and CD8<sup>+</sup>, respectively) cells. **d)** Normalized RNA  
862 expression levels of Prdm1 in PD-1<sup>-</sup>Tim-3<sup>-</sup> (n=3) and PD-1<sup>+</sup>Tim-3<sup>+</sup> (n=3) CD8<sup>+</sup> TILs  
863 (mean  $\pm$  s.e. is shown, \*\*\*p = 0.0004, two-sided t-test). **e)** Network model based on  
864 RNAseq gene expression data of naïve CD8<sup>+</sup> T cells from Prdm1<sup>fl/fl</sup> (WT) or  
865 CD4<sup>cre</sup>Prdm1<sup>fl/fl</sup> (Prdm1 cKO) mice stimulated in the presence of IL-27 and actual  
866 binding events (ChIPseq) data for Prdm1<sup>19</sup>. Green arrows designate genes up-regulated  
867 by Prdm1, red arrows designate genes down-regulated by Prdm1, and dashed gray arrows  
868 mark binding events.

869

870 **Extended Data Figure 7. Genomic tracks surrounding the co-inhibitory molecules**871 Lag3 **(a)**, Pd-1 **(b)**, Tigit **(c)** and Tim-3 **(d)** with overlay of Chipseq data of Prdm1<sup>16</sup> and

872 c-Maf<sup>19</sup> and ATACseq data of naïve CD4<sup>+</sup> cells induced with IL27 for 72h and ATACseq  
 873 data of CD8<sup>+</sup> T cells 27 days following chronic viral infection<sup>22</sup>. Regions of binding sites  
 874 common to both Prdm1 and c-Maf are indicated by the dotted rectangles. e) Luciferase  
 875 activity in 293T cells transfected with pGL4.23 luciferase reporters for depicted  
 876 enhancers of Tim-3 together with empty vector (control), constructs encoding Prdm1, c-  
 877 Maf, or both. Firefly luciferase activity was measured 48h after transfection and is  
 878 presented relative to constitutive Renilla luciferase activity.

879

880 **Extended Data Figure 8. Immune characterization of Prdm1 cKO, cMaf cKO, and**  
 881 **Prdm1/c-Maf cDKO before and after tumor challenge.**

882 **a)** Analysis of steady-state immune system in WT, c-Maf cKO, Prdm1 cKO, and  
 883 Prdm1/c-Maf cDKO. Summary data for CD4, CD8, Foxp3, CD44, CD62L, and CD69  
 884 expression in spleen from WT, c-Maf cKO, Prdm1 cKO and Prdm1/c-Maf cDKO mice.  
 885 Data are from biologically independent animals. mean  $\pm$  s.e.m is shown. \*p < 0.05; \*\*p  
 886 <0.01; \*\*\*\*p < 0.0001, one-way ANOVA and Tukey's multiple comparisons test. **b)** co-  
 887 inhibitory receptor expression in CD4<sup>+</sup> TILs from Prdm1/c-Maf cDKO mice. Top panels,  
 888 representative flow cytometry data from 3 independent experiments for TILs from WT  
 889 and Prdm1/c-Maf cDKO stained for PD-1, Tim-3, TIGIT, Pdpn, and Procr expression.  
 890 Bottom panels show summary data. Data are from biologically independent animals.  
 891 mean  $\pm$  s.e.m is shown \*p < 0.05, two-sided t-test. **c)** Top panels, representative flow  
 892 cytometry data from 3 independent experiments showing cytokine production from CD8<sup>+</sup>  
 893 TILs from WT and cDKO bearing B16F10 melanoma. Bottom panels, summary data.  
 894 Data are from biologically independent animals. mean  $\pm$  s.e.m is shown. \*p < 0.05, two-

895 sided t-test. **d)** Co-inhibitory receptor expression on CD8<sup>+</sup> TILs sorted from B16-OVA-  
896 bearing Rag1 KO mice that were transferred with Prdm1/c-Maf cDKO (n=4) or wild type  
897 (n=4) CD4<sup>+</sup> and CD8<sup>+</sup> T cells as indicated. Data are from biologically independent  
898 animals. mean  $\pm$  s.e.m is shown. \*P<0.05, one-way ANOVA and Tukey's multiple  
899 comparisons test. **e)** Rag1 KO mice were transferred with either wildtype or cDKO CD4<sup>+</sup>  
900 and CD8<sup>+</sup> (2:1 CD4:CD8 ratio) followed by subcutaneous injection of MC38-OVA. Mean  
901 tumor size  $\pm$  s.e.m is shown. \*\*\*\*P<0.0001, repeated measures ANOVA, Sidak's  
902 multiple comparisons test. On Day 14 post tumor implantation mice were sacrificed and  
903 TILs, spleen and draining Lymph nodes were harvested. **f)** The frequency of antigen  
904 specific CD8<sup>+</sup> T cells in the dLN of mice in (e).

905

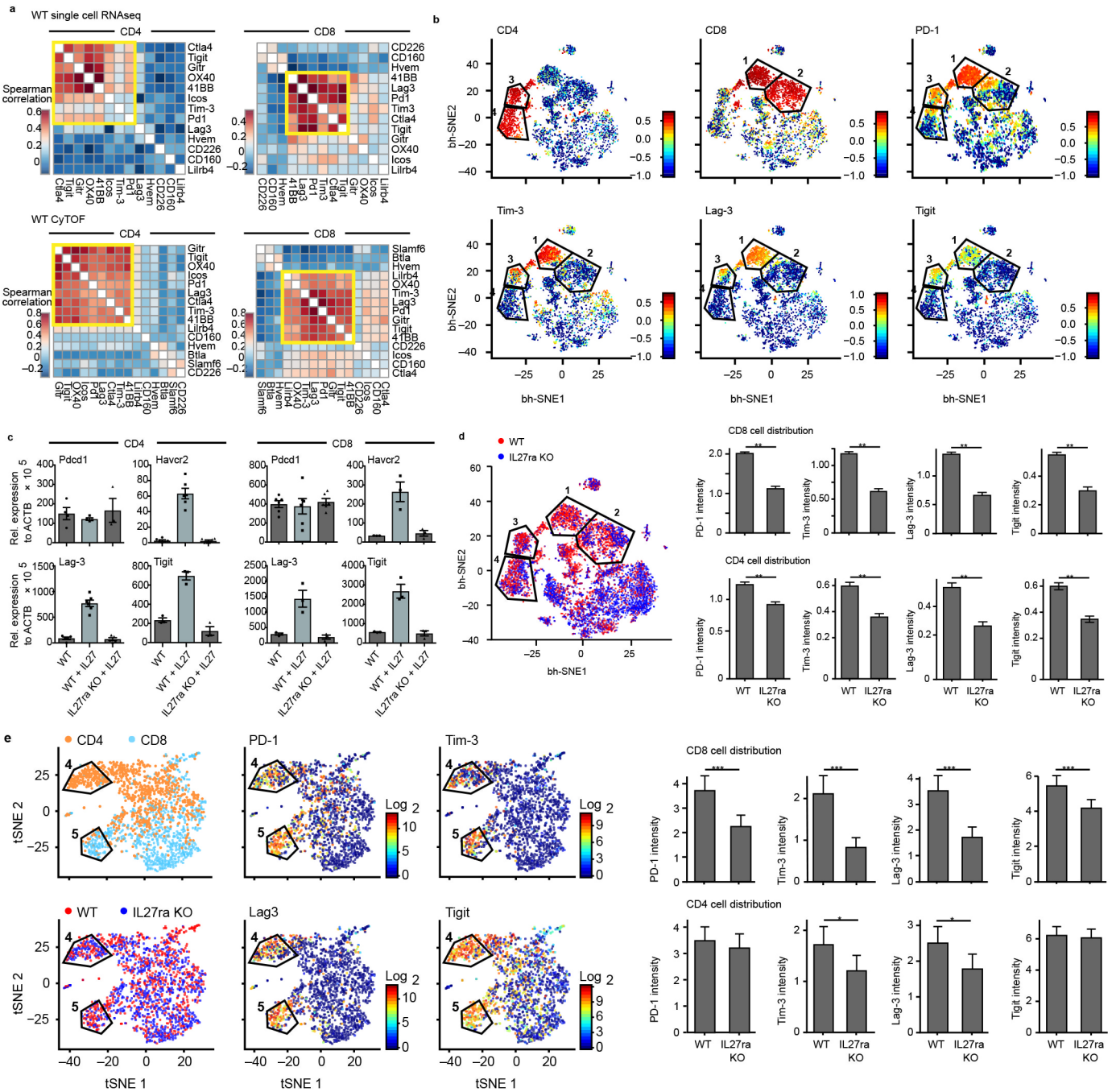
906 **Extended Data Figure 9. Examination of additive and non-additive (synergistic)**  
907 **effects of Prdm1 and c-Maf.**

908 **a)** A Heatmap showing all 940 DE genes between WT (n=5) and cDKO (Prdm1/c-Maf,  
909 n=4) and their expression in single KO (Prdm1 control n=7, Prdm1 KO n=3, cMaf  
910 control n=4 and cMaf KO n=3) mice. The red markings on the top of the heatmap  
911 indicate genes on whose expression the two knockouts have a statistically significant (p-  
912 value<0.05) non-additive effect in the cDKO (149 out of 940 DE genes). **b)** Volcano plot  
913 of the same analysis as in (a) for global gene expression. Genes whose expression in the  
914 two single knockouts have a statistically significant (p-value<0.05) non-additive effect in  
915 the cDKO (1144 out of 12,906 genes) and had abs (coefficient)>1 (779 out of 1144) are  
916 shown in orange.

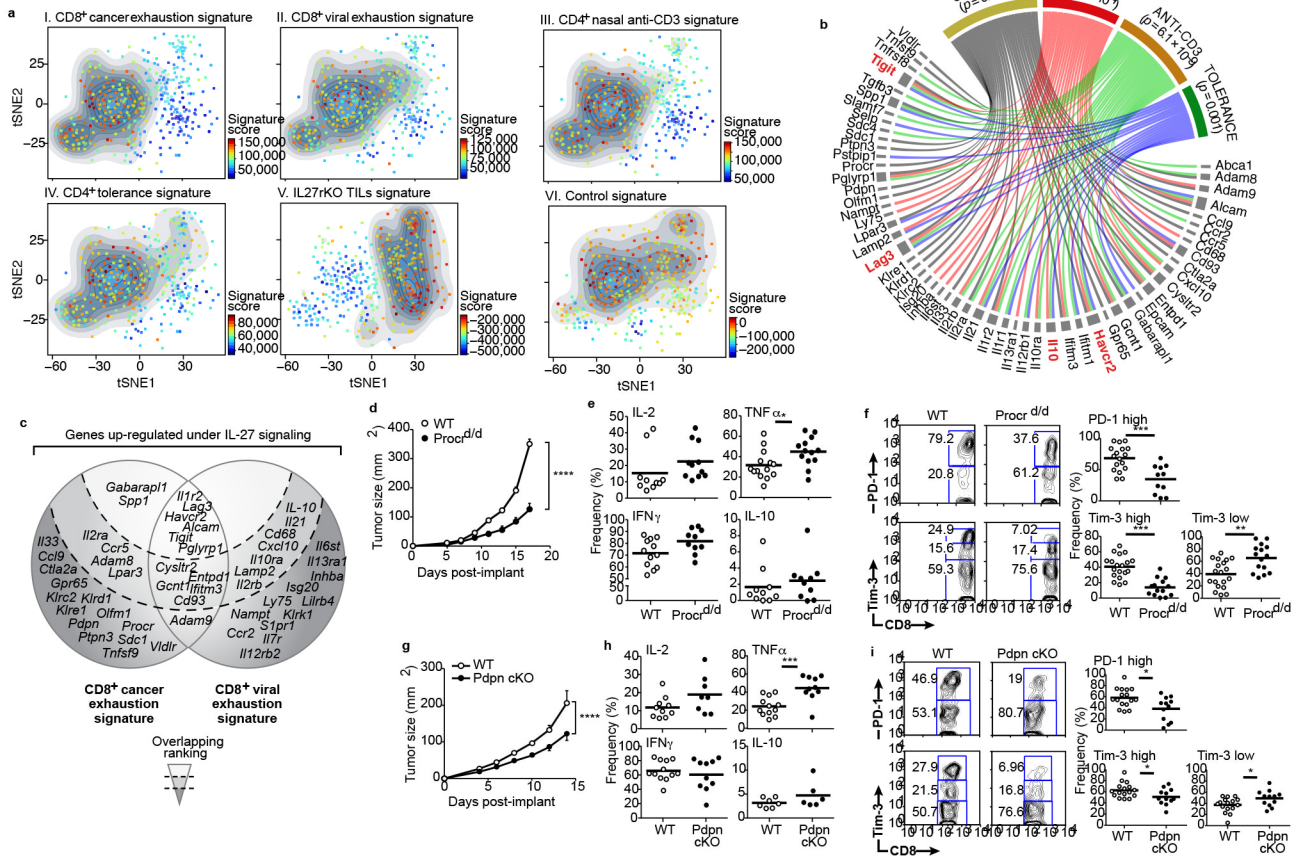
917



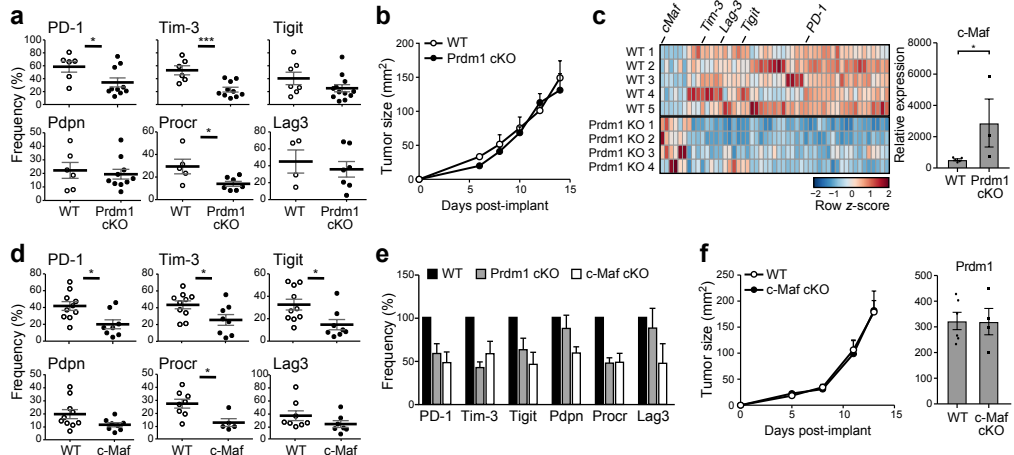
918 **Extended Data Figure 10. Comparison of gene expression between Prdm1/c-Maf**  
919 **cDKO TILs and CD8<sup>+</sup> TILs populations from wild type mice. a)** Barcode enrichment  
920 plot displaying two gene sets in a ranked gene list. The ranked gene list was defined as  
921 fold change in gene expression between Prdm1/c-Maf cDKO and WT CD8<sup>+</sup> TILs. The  
922 three gene sets consist of differentially expressed genes between: PD-1<sup>+</sup>Tim-3<sup>+</sup> CD8<sup>+</sup>  
923 (DP, n=3) and PD-1<sup>-</sup>Tim-3<sup>-</sup> CD8<sup>+</sup> (DN, n=3) TILs, PD-1<sup>+</sup>Tim-3<sup>+</sup> CD8<sup>+</sup> (DP) TILs and  
924 Memory CD8<sup>+</sup> (n=3), and PD-1<sup>+</sup>Tim-3<sup>-</sup> CD8<sup>+</sup> (SP, n=3) and PD-1<sup>-</sup>Tim-3<sup>-</sup> CD8<sup>+</sup> (DN)  
925 TILs. **b)** This analysis was followed by four statistical tests (one-sample Kolmogorov-  
926 Smirnov test, mean-rank gene set test (wilcoxGST), hypergeometric, and competitive  
927 gene set test accounting for inter-gene correlation) for enrichment of these signatures in  
928 the cDKO expression profile. **c)** WT versus cDKO volcano plot. Green indicates genes  
929 that were up-regulated in the PD-1<sup>-</sup>Tim-3<sup>-</sup> CD8<sup>+</sup> (DN) TILs and red indicates genes that  
930 were up-regulated in the PD-1<sup>+</sup>Tim-3<sup>+</sup> CD8<sup>+</sup> (DP) TILs. **d)** WT versus cDKO volcano  
931 plot. Red indicates genes that were up-regulated in PD-1<sup>+</sup>CXCR5<sup>+</sup>CD8<sup>+</sup> T cells and green  
932 indicates genes that were up-regulated in PD-1<sup>+</sup>CXCR5<sup>-</sup>CD8<sup>+</sup> T cells in chronic LCMV  
933 infection<sup>23</sup>. **e).** A tSNE plot of the 588 CD8<sup>+</sup> TILs harvested from WT mice bearing  
934 B16F10 melanoma tumors, colored by the relative signature score for the co-inhibitory  
935 module (272 genes, **Supplementary Information Table 2**), the cDKO signature (shown  
936 in (g)), and the PD-1<sup>+</sup>CXCR5<sup>+</sup>CD8<sup>+</sup> T cell signature from chronic virus infection<sup>23</sup>. The  
937 contour plot marks the region of highly scored cells by taking into account only those  
938 cells that have a signature score above the mean.  
939  
940

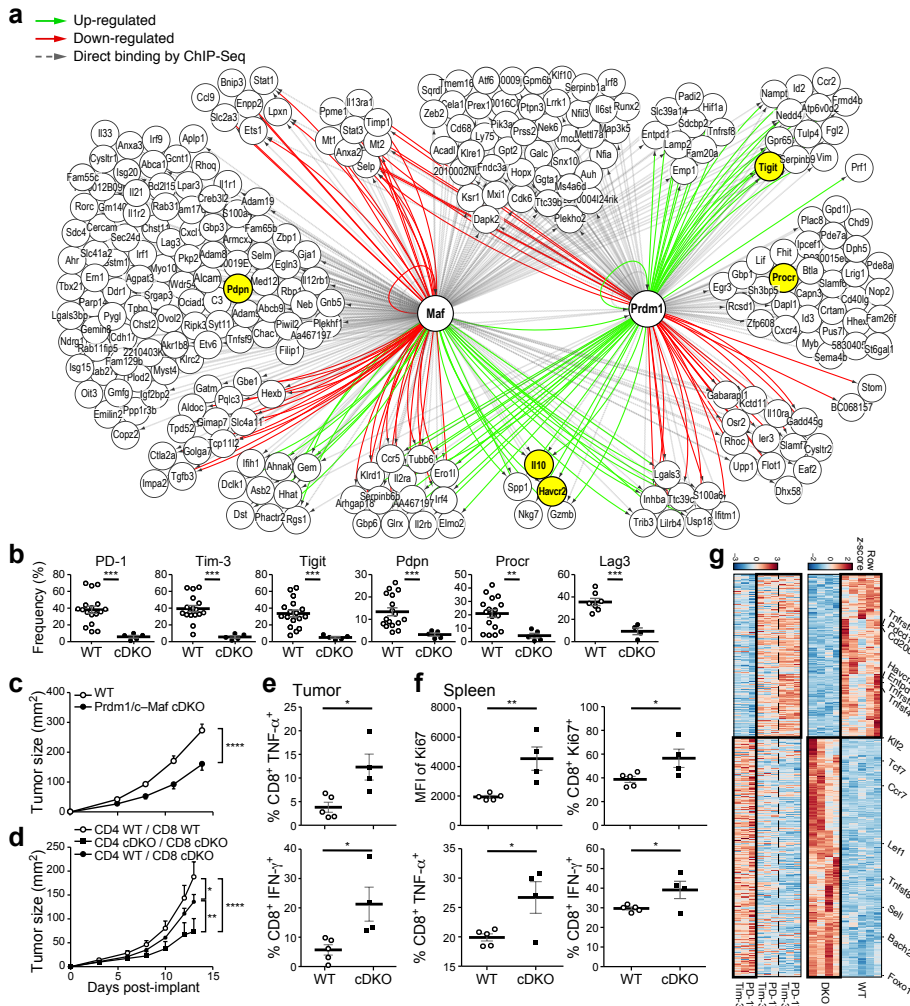


180mm X 178mm



170mm X 117mm





120mm X 133mm